Journal of Power Sources 267 (2014) 329–336

Contents lists available at ScienceDirect

Journal of Power Sources

journal homepage: www.elsevier.com/locate/jpowsour

The reaction mechanism of SnSb and Sb thin film anodes for Na-ion batteries studied by X-ray diffraction, ^{119}Sn and ^{121}Sb Mössbauer spectroscopies

Loïc Baggetto [a, *], Hien-Yoong Hah [b, c], Jean-Claude Jumas [d], Charles E. Johnson [b], Jacqueline A. Johnson [c], Jong K. Keum [e], Craig A. Bridges [f], Gabriel M. Veith [a, *]

[a] Materials Science and Technology Division, Oak Ridge National Laboratory, Oak Ridge, TN 37831, USA
[b] Center for Laser Applications, University of Tennessee Space Institute, Tullahoma, TN 37388, USA
[c] Department of Mechanical, Aeronautical and Biomedical Engineering, University of Tennessee Space Institute, Tullahoma, TN 37388, USA
[d] Institut Charles Gerhardt, Université Montpellier II, 34095 Montpellier Cedex 5, France
[e] Neutron Science Directorate, Spallation Neutron Source, Oak Ridge National Laboratory, Oak Ridge, TN 37831, USA
[f] Chemical Sciences Division, Oak Ridge National Laboratory, Oak Ridge, TN 37831, USA

HIGHLIGHTS

- SnSb and Sb thin films are studied as anode materials for Na-ion batteries.
- Local environments are compared to powder model compounds.
- Crystallization into Na_3Sb occurs at higher temperatures (65 and 95 °C).

ARTICLE INFO

Article history:
Received 15 February 2014
Received in revised form
3 May 2014
Accepted 17 May 2014
Available online 2 June 2014

Keywords:
Sodium ion anode
Tin antimony (SnSb)
Antimony (Sb)
X-ray diffraction (XRD)
^{119}Sn Mössbauer spectroscopy
^{121}Sb Mössbauer spectroscopy

ABSTRACT

The electrochemical reaction of Sb and SnSb anodes with Na results in the formation of amorphous materials. To understand the resulting phases and electrochemical capacities we studied the local order using ^{119}Sn and ^{121}Sb Mössbauer spectroscopies in conjunction with measurements performed on model powder compounds of Na–Sn and Na–Sb to further clarify the reactions steps. For pure Sb the sodiation starts with the formation of an amorphous phase composed of atomic environments similar to those found in NaSb, and proceeds further by the formation of crystalline Na_3Sb. The reversible reaction takes place during a large portion of the charge process. At full charge the anode material still contains a substantial fraction of Na, explaining the lack of recrystallization into crystalline Sb. The reaction of SnSb yields Na_3Sb at full discharge at higher temperatures (65 and 95 °C) while the RT reaction yields amorphous compounds. The electrochemically-driven, solid-state amorphization reaction occurring at RT is governed by the simultaneous formation of Na-coordinated Sn and Sb environments, as monitored by the decrease (increase) of the ^{119}Sn (^{121}Sb) Mössbauer isomer shifts. Overall, the monitoring of the hyperfine parameters enables to correlate changes in Na content to the local chemical environments.

1. Introduction

Recently, there has been a tremendous focus on the exploration of materials that could be suitable Na-ion anodes [1–14]. Of all these studies elemental Sn [1–3] and Sb [4,5] are the most widely studied due to their large theoretical storage capacities, 847 and 660 mAh g^{-1}, respectively. Interestingly, structures of the electrochemical Na–Sn and Na–Sb intermediates and final phases differ significantly from the products formed during the reaction with Li [2–5]. Intermetallic compounds offer several advantages compared to their parent counterparts such as improved cycle-life and rate performance [6–13] coupled with less drastic volume changes. Of all the intermetallics, SnSb possess the highest theoretical capacity of 752 mAh g^{-1}. Recent *in situ* X-ray diffraction (XRD) studies by Darwiche et al. reported that SnSb remains amorphous at all

* Corresponding authors.
E-mail addresses: loic_baggetto@yahoo.fr (L. Baggetto), veithgm@ornl.gov (G.M. Veith).

http://dx.doi.org/10.1016/j.jpowsour.2014.05.083
0378-7753/

potentials during the reaction with Na [6]. The lack of long range order makes it difficult to identify the reaction mechanisms and predict new anode chemistries which may exhibit optimal performances.

While there are a variety of methods available to study local order, such as nuclear magnetic resonance, pair distribution function or X-ray absorption spectroscopy, this work focuses on the use of Mössbauer spectroscopy. Mössbauer spectroscopy relies on the recoil-free resonant absorption of gamma rays by the nuclei of specific Mössbauer active isotopes, such as ^{119}Sn and ^{121}Sb, and is particularly powerful at elucidating the chemical environment of the probed atom. This technique has shown to be highly accurate at resolving the reaction mechanism of Sb- [11,14] and Sn-based [15–18] electrodes for lithium-ion batteries, in particular SnSb [16].

In the present work, we have employed Sb and SnSb thin films as model electrodes to investigate the local bonding and reaction mechanisms with respect to Na. Thin films are particularly useful to address these issues since there are no binders or additives employed, which can enable the understanding of the intrinsic properties of the material. We have revisited the reaction mechanism of SnSb with Na using XRD, for electrodes prepared at room temperature and at higher temperatures (65 and 95 °C). We report for the first time the reaction mechanism of SnSb using ^{119}Sn and ^{121}Sb Mössbauer spectroscopies. These studies are also supported by investigations of the reaction of pure Sb with Na using ^{121}Sb Mössbauer spectroscopy along with reference Na–Sb and Na–Sn compounds prepared by solid state synthesis.

2. Experimental

2.1. Samples preparation

SnSb films of various thicknesses were deposited on roughened Cu foils using DC magnetron sputtering of a homemade target in pure Ar (99.99%, Air Liquide) at 20 m Torr pressure and 20 W DC power. The homemade target was prepared by ball-milling pure Sb (99.5%, Sigma–Aldrich) and Sn (99.9%, Alfa Aesar) powders with yittria-stabilized zirconia balls, pressing the recovered powder into a 2″ diameter disk, and annealing at 200 °C in flowing Ar for 40 h. Sb films were prepared using a homemade Sb target and conditions reported earlier [4]. Film thickness was estimated using a quartz microbalance installed inside the chamber. The thickness was calculated based on the weight of the samples measured using a Mettler balance with 10 μg precision and the expected density of SnSb of 6.95 g cm^{-3}. After preparation, the samples were stored inside an Ar-filled glovebox.

Reference powders of NaSb, Na_3Sb and Na–Sn model compounds was prepared inside an Ar-filled glovebox by adding and reacting stoichiometric amounts of Na (ACS reagent, Sigma–Aldrich) and ball-milled Sb (99+ %, Alfa Aesar) or as-received Sn (99.8%, Alfa Aesar) powders inside homemade Al foil crucibles placed inside a Pyrex tube. Using a Swagelok fitting connected to a vacuum valve, a primary static vacuum was created inside the tube. Subsequently, the tube was placed in an oven at 175 °C for several hours. As soon as the Na melted, it reacted with Sb to form a solid compound. The recovered powder was ground thoroughly, pressed into a pellet and further annealed at 175 °C or 300 °C in Ar. This procedure was repeated to ensure good homogeneity of the compound.

2.2. Experimental characterization

Electrochemical characterization was conducted at 25 °C inside a thermostatic incubator using 2-electrode coin cells (2032 hardware, Hohsen) prepared inside an Ar-filled glovebox. The cells consisted of pure Na as counter electrode, the thin film sample as working electrode and two pieces of glass fiber separator impregnated by 1 M $NaClO_4$ in anhydrous propylene carbonate (PC, Sigma–Aldrich) electrolyte solution. Electrochemical preparation was performed on a Maccor 4000 series. Short-circuited cells (48 h) were also prepared at various temperatures for XRD characterization. For XRD and Mössbauer spectroscopy experiments, the samples were extracted from coin cells inside an Ar glovebox, pressed onto fiber paper to remove the excess of electrolyte, conditioned and sealed under Ar inside heat-sealed pouch bags.

A Bruker D8 Advance diffractometer with a MoKα source, Zr filter and scintillation detector was used for XRD collection of Na–Sb and Na–Sn powders. The powders were finely ground, loaded inside a 0.5 mm glass capillary, which was temporarily sealed with vacuum grease inside the glovebox then heat-sealed with a methane–oxygen torch outside the glovebox. Data were collected using a step size of 0.02° 2θ, and typically over a range of 5° to 40° 2θ, on samples in spinning capillaries to minimize preferred orientation effects and improve particle statistics. XRD patterns of electrodes were collected with a PANalytical X'Pert Pro MPD diffractometer with a CuKα source, Ni filter and X'Celerator detector for measurements on samples sealed with Kapton tape (25 μm) onto a glass slide. Scans were limited to no more than 45 min to ensure that no reaction occurred in air.

For Mössbauer experiments, 4 to 6 thin film samples of 2.5–4 μm, equivalent to about 20–30 mg, were prepared for each electrochemical position to provide enough signal. ^{119}Sn transmission Mössbauer spectroscopy was acquired at room temperature in the constant acceleration mode using components manufactured by ORTEC and WissEl. The source used for these experiments was ^{119m}Sn embedded in a $CaSnO_3$ matrix. The velocity scale was calibrated with the magnetic sextet of a high-purity α-Fe foil absorber exposed to a Rh^{57}Co source. The spectra were fitted to Lorentzian profiles by the least-squares method. ^{119}Sn isomer shifts are given with respect to the room temperature spectrum of $BaSnO_3$.

^{121}Sb transmission Mössbauer spectroscopy was recorded in the constant acceleration mode using a system manufactured by SEE Co., Edina, MN. The source was 100 μCi of ^{121m}Sn in $BaSnO_3$ at room temperature, and a Xe–CH_4 proportional counter was used to detect the sum of the 37.2 keV γ-rays and 8 keV escape peak. Most samples were cooled to 6 K under vacuum in a closed-cycle cryogen-free refrigerator (Janis, Wilmington, MA and SEE Co.), to increase the Mössbauer fraction and suppress the materials oxidation. Few samples were measured at 20 or 70 K; the change in isomer shift due to a second order Doppler shift from 70 to 6 K is small and can be estimated to be significantly less than 0.05 mm s^{-1} for ^{121}Sb [19]. The velocity scale was calibrated with a high-purity α-Fe foil absorber exposed to a Rh^{57}Co source. The spectra were fitted with a custom Mössbauer program using an 8-line Lorentzian profile [20]. ^{121}Sb isomer shifts are given with respect to the source at room temperature.

Surface chemistry was probed using a PHI 3056 X-ray photoelectron spectrometer (XPS) equipped with AlKα and MgKα sources (1486.6 and 1253.6 eV) at a measurement pressure below 10^{-8} Torr. Samples were transferred to the XPS chamber using an airtight vacuum transfer system. High-resolution scans were acquired at 350 W with 23.5 eV pass energy and 0.05 eV energy step. Survey scans were measured at 350 W with 93.9 eV pass energy and 0.3 eV energy steps. The binding energies were shifted by setting the strongest carbon signal to 284.8 eV to account for charging. The intensities of the presented spectra are not normalized and are simply shifted vertically for clarity.

3. Results and discussion

3.1. Starting films properties

The morphology of SnSb thin films deposited onto Cu roughened foil is presented in Fig. 1a. The films are composed of agglomerated nanoparticles following the rough morphology of the Cu substrate. The grains show sharp features with the size of the individual particles well below 1 μm. The structure of the thin films is characterized by XRD (Fig. 1b) while the surface chemistry was characterized using XPS (Fig. S1). The crystal structure of 'SnSb' was revisited several years ago and found to be incommensurately modulated with an underlying rhombohedral parent structure adopting an R-3m symmetry [21]. As seen in Fig. 1b, the crystalline films share the same R-3m structure and exhibit a strong (101) preferred orientation (peak at $2\theta \sim 29°$). Rietveld refinements (Fig. S2) yield lattice parameters of $a = b = 4.3348$ (2) Å and $c = 5.3545$ (2) Å. A very small peak (^) around $2\theta = 46.5°$ has been systematically measured on all films and may either result from an impurity or the presence of a satellite peak resulting from the SnSb incommensurate structure [21]. The surface of the thin film material is characterized by the presence of Sb and Sn native oxides covering the metallic film (Fig. S1). The presence of the metallic bonds is clearly observed in the 3d and 4d spectra of Sn and Sb as evident in the low binding energy peaks near 528 and 31.3 eV for Sb and 485 and 23.7 eV for Sn. The surface oxides are evidenced by the O1s data (note that O1s overlaps with Sb3d5/2 of the Sb oxide) and the peaks observed at higher energies relative to the metallic peaks described above.

The electrochemical profiles of the electrode measured are presented in Fig. 2. The profiles consist of three major features during charging and discharging, as reported earlier on powder electrodes [6]. The profiles during the first and second charge are nearly identical, however, the beginning of the first discharge is significantly different from that of the second. Plateaus/slopes are centered on 0.51, 0.37 and 0.05 V during the first discharge, and 0.17, 0.58 and 0.82 V during charging. During the next sodiation cycle the flat plateau originally present at 0.51 V is replaced by a plateau around 0.64 V followed by a discharge profile quasi-identical to the initial cycle. This difference can be related to the difference in structure between the cycled and starting material. The starting material is crystalline, leading to a flat voltage plateau at 0.51 V during the first discharge whereas the cycled material is amorphous [6] and is characterized by a voltage slope. It is clear that the capacity spent on the slope, around 0.64 V, present during the second cycle is much smaller than that spent on the first plateau, which is related to two loss processes. First, the electrolyte decomposition, which leads to the formation of an SEI layer, consumes additional charge during the first discharge. Moreover, the removal of Na from the electrode may not be complete during the first charge, as observed from the lower than expected storage capacity. The reversible formation of $Na_{15}Sn_4$ and Na_3Sb from SnSb corresponds to a theoretical capacity of 752 mAh g^{-1} whereas the maximum reversible capacity at these very low currents is about 700 mAh g^{-1}. The lower than expected removal of Na has been widely observed on Sb-based electrodes [5–7,9–13] including SnSb [6].

The changes in structure investigated by XRD are presented in Fig. 3. The crystalline structure of the electrode is converted to an amorphous phase after the completion of the first discharge plateau (0.51 V). The electrode structure remains amorphous during discharge and charge, as evidenced by the absence of sharp

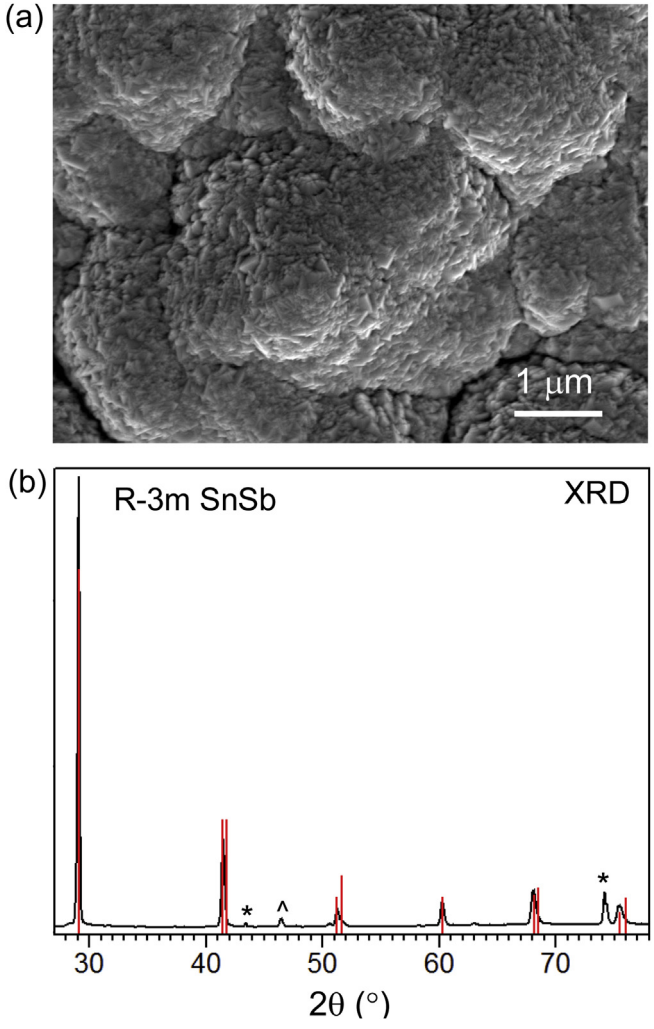

Fig. 1. Properties of the starting thin film material. (a) Surface morphology imaged by SEM of the pristine SnSb thin film material deposited onto roughened Cu foil. (b) XRD pattern of the pristine SnSb thin film material including the reference pattern for SnSb. (*) indicate the diffraction lines from the Cu foil.

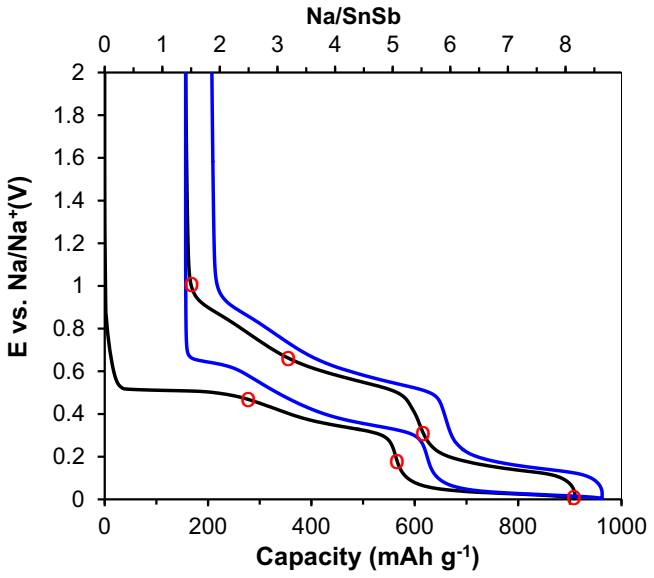

Fig. 2. Electrochemical potential profiles of SnSb thin film (1 μm) electrodes during the first two cycles using a current density of 12 μA cm^{-2} (C/50).

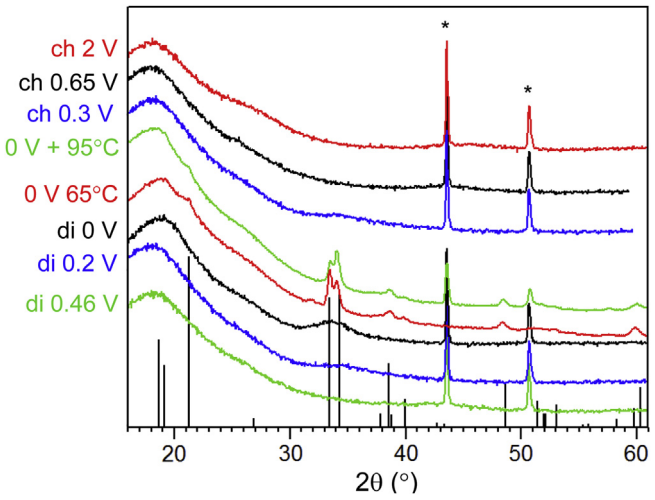

Fig. 3. Structural characterization of SnSb thin film electrodes at various electrode potentials by XRD. The broad hump at low angles results from the Kapton tape used to protect the electrodes from air during the measurement. For the discharge position at 0 V, electrodes were short circuited for 48 h at room temperature (di 0 V, black) or at 65 °C (0 V 65 °C, red). In addition, an electrode short circuited for 48 h at room temperature was post-annealed in Ar at 95 °C (0 V RT + 95 °C, green). Vertical black bars are for Na_3Sb reference pattern. (*) indicate the diffraction lines of the Cu foil. (For interpretation of the references to color in this figure legend, the reader is referred to the web version of this article.)

diffraction peaks for electrodes prepared at 25 °C. In addition, the growth of a broad hump is observed around $2\theta = 34°$, which suggests the formation of an amorphous/nanocrystalline phase, such as possibly Na_3Sb or some Na_xSn phases. A short-circuited cell (0 V) was placed in an oven at 65 °C to enhance the reaction kinetics, particularly solid-state diffusion, and allow a maximum supply of Na to the SnSb electrode. It is interesting to observe that the corresponding XRD pattern displays diffraction lines for the hexagonal Na_3Sb (P63/mmc) phase at the location where broad humps have been measured for electrodes prepared at 25 °C. The change in structure was further studied at higher temperature for an electrode of a cell short-circuited at room temperature and post-annealed in Ar at 95 °C. The corresponding XRD pattern shows diffraction lines for Na_3Sb only.

These results confirm that the atomic diffusion within the Na–Sn–Sb nanocomposite is insufficient to achieve long-range crystallization of Na_3Sb at room temperature. Moreover, in contrast to the formation of Na_3Sb nanocrystalline domains, there is no evidence for the formation of Na_xSn clusters at higher temperature. This is rather unexpected given that several crystalline Na_xSn phases ($x = 2.35$ or $x = 3.75$) can be electrochemically formed during the reaction of pure Sn with Na at 25 °C [1–3]. The crystallization into the phase of composition $Na_{2.35}Sn$ should be achievable here since that the total reversible capacity exceeds 5.35 Na/SnSb (Fig. 2). Given that the electrochemical formation of Na_xSb phases occurs at a much more positive electrode potential [4,5] than for Na_xSn compounds [2,3], it might be that the reaction of SnSb proceeds by the extrusion of Sn at the grain boundaries of growing Na_xSb domains. The absence of crystallization of Na_xSn compounds might thereby result from the formation of Na_xSb nanodomains embedded in a Na_xSn nanomatrix, which possesses a restricted spatial dimension preventing crystallization. It could also be that the internal strain is sufficient to prevent the formation of crystalline Na_xSn nanodomains. Annealing at higher temperatures can favor the motion of Na atoms within the Na_xSb and Na_xSn domains, however, these temperatures are likely insufficient to promote the coalescence of the Na_xM (M = Sb, Sn) domains, particularly those of Na_xSn, to ensure a long-range structure crystallization. Further discussion for the evidence of the formation of Na_xSn domains of very small dimensions (few nanometers) will be provided in relation to the discussion of the quadrupole splitting of ^{119}Sn Mössbauer spectra.

The reaction of pure Sb thin films studied by ^{121}Sb Mössbauer spectroscopy will be discussed next (Fig. 4). This discussion is important as it supports the discussion of the reaction mechanism of SnSb. The Mössbauer spectra measured at various electrochemical positions (Fig. 4a) are presented in Fig. 4b with corresponding isomer shifts given in Table 1. During discharge (sodiation), the Sb environment characterized by an isomer shift of −11.85 mm s^{-1} evolves into two environments characterized by signals around −11.2 mm s^{-1} and −8.0 mm s^{-1}. We attribute these responses to the two asymmetric Sb sites in monoclinic NaSb (Fig. 5a, Figs. S3a and S4, Table S1). The latter value around −8.0 mm s^{-1} also matches that expected for the environment of Sb inside hexagonal Na_3Sb (−7.95 mm s^{-1}, c.f. Fig. 5b and

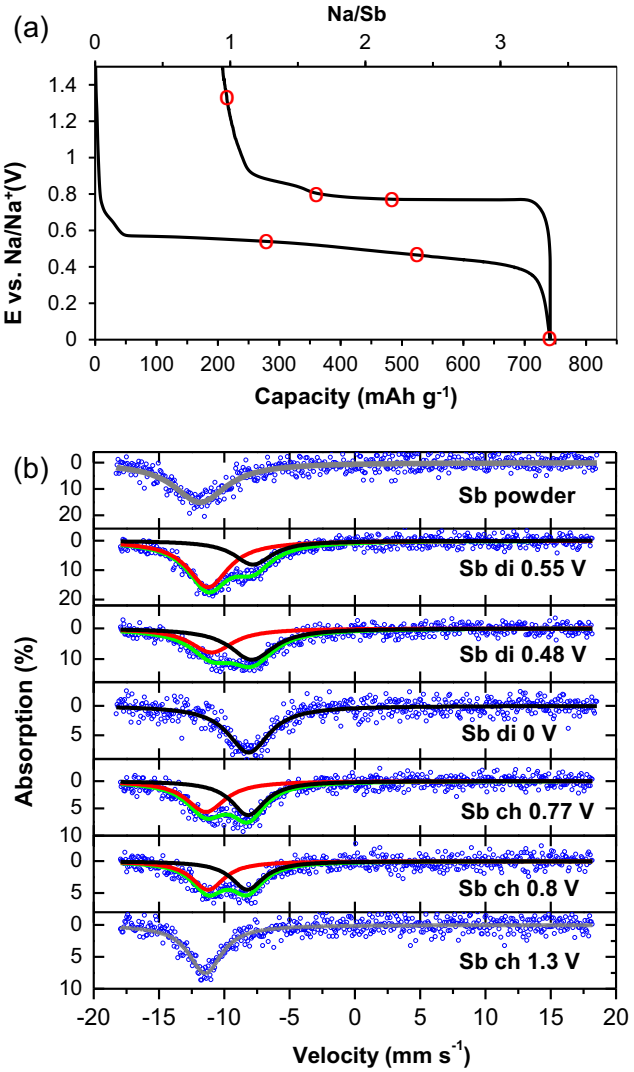

Fig. 4. Characterization of the reaction of pure Sb with Na using ^{121}Sb Mössbauer spectroscopy. (a) Electrochemical profile of Sb during the first cycle and (b) corresponding ^{121}Sb Mössbauer spectra measured at the positions highlighted by markers in (a). Red and black sub-spectra are for NaSb-like and Na_3Sb-like environments. (For interpretation of the references to color in this figure legend, the reader is referred to the web version of this article.)

Table 1
^{121}Sb Mössbauer isomer shifts (δ) for Sb sites in Sb and SnSb electrodes during the reaction with Na, and for powder samples. Values result from fitting the Mössbauer spectra (Figs. 4 and 6 and Fig. S3) using Lorentzian functions.

Sample	δ_1 (mm s^{-1})	δ_2 (mm s^{-1})
Sb powder	−11.85	–
Sb discharge 0.55 V	−11.21	−7.78
Sb discharge 0.48 V	−10.95	−7.86
Sb discharge 0 V	–	−8.11
Sb charge 0.76 V	−11.39	−8.15
Sb charge 0.8 V	−11.22	−8.21
Sb charge 1.3 V	−11.44	–
SnSb powder	−10.69	–
SnSb discharge 0.46 V	−10.41	–
SnSb charge 0.2 V	–	−8.20
SnSb discharge 0 V	–	−8.10
SnSb charge 0.3 V	−9.72	−7.80
SnSb charge 0.65 V	−10.12	–
SnSb charge 1 V	−10.38	–
NaSb powder	−11.59	−8.33
Na_3Sb powder	−7.95	–

Figs. S3b and S4, Table S2) [9]. This result is also in very good agreement with the value reported by Kitadai et al. [22] when assuming an isomer shift of −8.6 mm s^{-1} for InSb with respect to the source [23]. The absence of crystallization in NaSb is possibly due to the slow atomic mobility preventing the arrangement into the somewhat complex monoclinic structure (Fig. 5a). Upon further sodiation, the environment with less Na is converted to a richer in Na environment, as evident from the increase in isomer shift [9], until only the single Sb environment present in Na_3Sb (Fig. 5b) is measured. When the conversion is complete the atomic arrangement crystallizes into the somewhat less complex hexagonal Na_3Sb structure [4,5]. During charge (desodiation), two Sb environments similar to those found during discharge are measured. The environment at −8.0 mm s^{-1} eventually vanishes at full charge (1.3 V) and only the response for a Na_xSb ($x < 1$) compound is measured at −11.44 mm s^{-1}. The more positive isomer shift compared to pure Sb (−11.85 mm s^{-1}) suggests the lack of full desodiation [11,14–18] or the formation of a disordered Sb structure, which both could explain why the electrode material does not crystallize back into Sb R-3m structure. The lower than theoretical reversible capacity measured for pure Sb, however, supports the absence of full desodiation [4,5].

The properties of SnSb thin films have been subsequently studied using ^{121}Sb Mössbauer spectroscopy (Fig. 6, Table 1). The starting material is characterized by a ^{121}Sb isomer shift of about −10.69 mm s^{-1}. When SnSb is discharged to 0 V then charged to 1 V, the isomer shift increases then decreases to −10.38 mm s^{-1}. The more positive isomer shift compared to SnSb suggests that Na remains in the structure at 1 V [11,14–18], as expected from the lower than theoretical storage capacity (Fig. 2) and the reaction mechanism of pure Sb (Fig. 4). During sodiation (discharge), the evolution of the isomer shift suggests that most of the reaction between Sb in SnSb and Na occurs during the discharge step comprised between 0.46 and 0.2 V, and that hardly any reaction

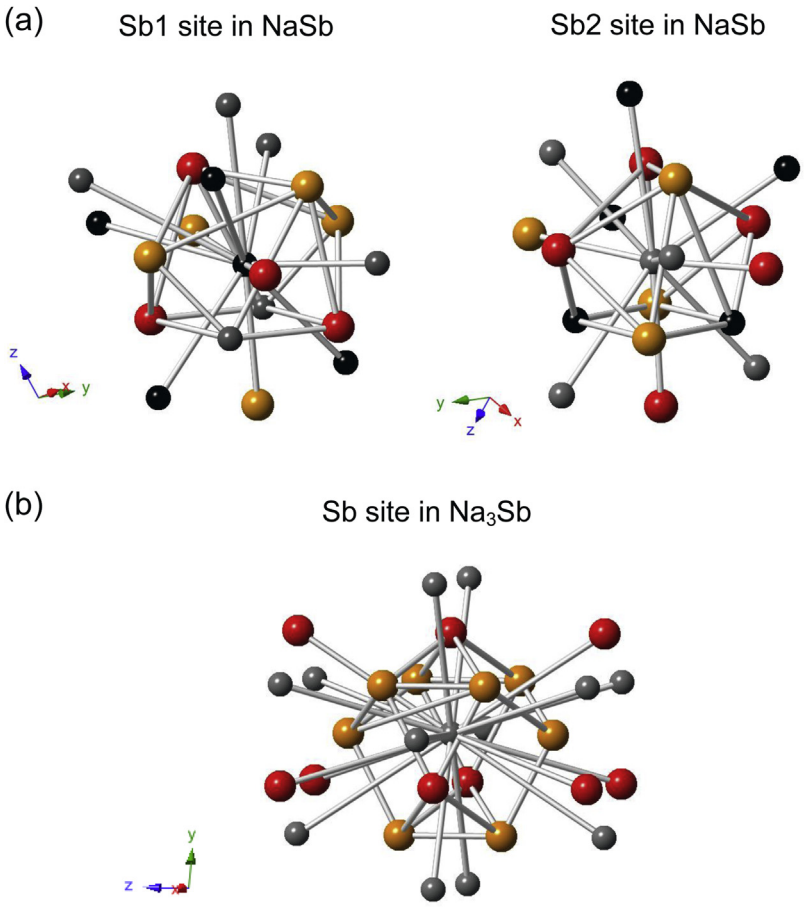

Fig. 5. Local atomic environments of Sb atoms in (a) monoclinic NaSb (P21/c) and in (b) hexagonal Na_3Sb (P63/mmc). Black and gray balls in NaSb are for Sb1 and Sb2 sites, respectively. Gray balls in Na_3Sb are for Sb. Orange and red balls are for Na sites. (For interpretation of the references to color in this figure legend, the reader is referred to the web version of this article.)

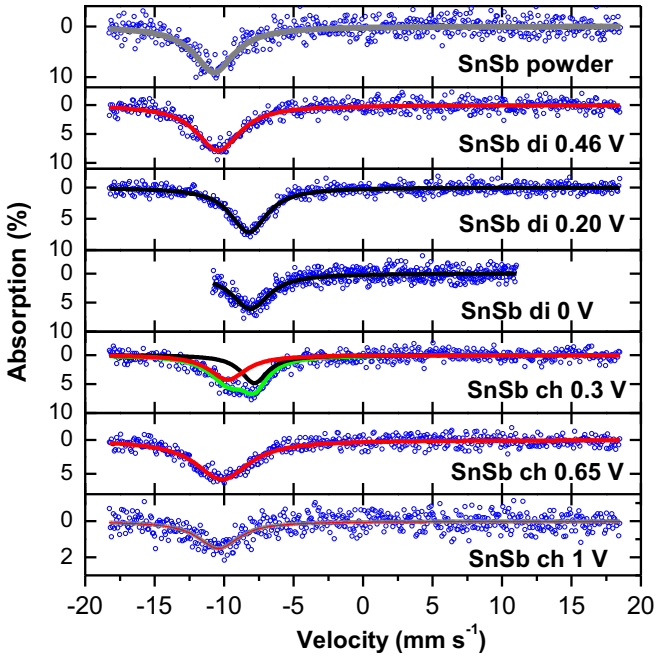

Fig. 6. Characterization of the reaction of SnSb with Na using ^{1}21Sb Mössbauer spectroscopy, corresponding to the positions highlighted by markers in Fig. 2.

occurs between Sb and Na below 0.2 V. During charge (desodiation), the changes are more gradual and the reaction behaves similarly to the reaction of pure Sb with Na, suggesting the segregation of Sb and Sn during the first discharge process.

The reaction of SnSb thin films studied by ^{119}Sn Mössbauer spectroscopy is discussed next. During discharge (sodiation), the reaction is characterized by a decrease of the ^{119}Sn isomer shift from the environment expected for SnSb into more negative isomer shifts (Fig. 7a, Table 2). At 0.46 V, an average isomer shift response of 2.34 mm s^{-1} is measured. This spectrum shows a broad line corresponding to an unresolved quadrupole doublet of

Table 2
^{119}Sn Mössbauer hyperfine parameters (isomer shift δ, quadrupole splitting Δ and line width Γ) for SnSb electrodes during the reaction with Na, resulting from fitting the Mössbauer spectra (Fig. 7) using Lorentzian functions.

Sample	δ (mm s^{-1})	Δ (mm s^{-1})	Γ (mm s^{-1})
SnSb	2.65 (3)	0.36 (5)	0.83 (5)
Discharge 0.46 V	2.34 (1)	0.71 (2)	1.00 (1)
Discharge 0.2 V	2.30 (2)	0.53 (3)	1.00 (4)
Discharge 0 V	2.25 (3)	0.53 (2)	1.05 (3)
Charge 0.3 V	2.28 (3)	0.53 (3)	1.00 (4)
Charge 0.65 V	2.35 (2)	0.54 (2)	0.99 (4)
Charge 1 V	2.42 (2)	0.49 (4)	1.10 (5)

0.71 mm s^{-1}. This large value indicates a fair amount of local coordination asymmetry around Sn atoms. Upon further sodiation, the isomer shift decreases to 2.30 mm s^{-1} at 0.2 V and 2.25 mm s^{-1} at 0 V, accompanied with somewhat lower, yet relatively large, quadrupole splitting values which indicate a fair amount of local atomic asymmetry around Sn. The decrease of the isomer shift is consistent with the increase in Na content, as measured on Na–Sn model compounds ([3]) or for Sn during the electrochemical reaction with Na [2] or Li [15–18]. The maximum sodiation of SnSb is represented by an isomer shift of 2.25 mm s^{-1}, which is larger than what is measured for fully sodiated Sn films [2,3] or for $Na_{15}Sn_4$ model compound [3] with a value around 2.15–2.18 mm s^{-1}. This can suggest that the sodiation of Sn atoms in SnSb is not as pronounced as in pure Sn and may partly explain why the reversible capacity is lower than theoretical.

The reaction during charge (desodiation) is now be discussed (Fig. 7b, Table 2). The charge is characterized by an increase of the average isomer shift to 2.28, 2.35 and 2.42 mm s^{-1} for 0.3, 0.65 and 1 V, respectively. It is interesting to observe that the isomer shift values during discharge to 0.46 V and charge to 0.65 V are almost equal (2.34 and 2.35 mm s^{-1}), similar to the electrodes during discharge to 0.2 V and charge to 0.3 V (2.30 and 2.28 mm s^{-1}), which can be related to the similar compositions of the electrodes (Fig. 2a). The electrode charged to 1 V has a more positive isomer shift, which is, however, significantly more negative than that of the starting material (2.65 mm s^{-1}). This

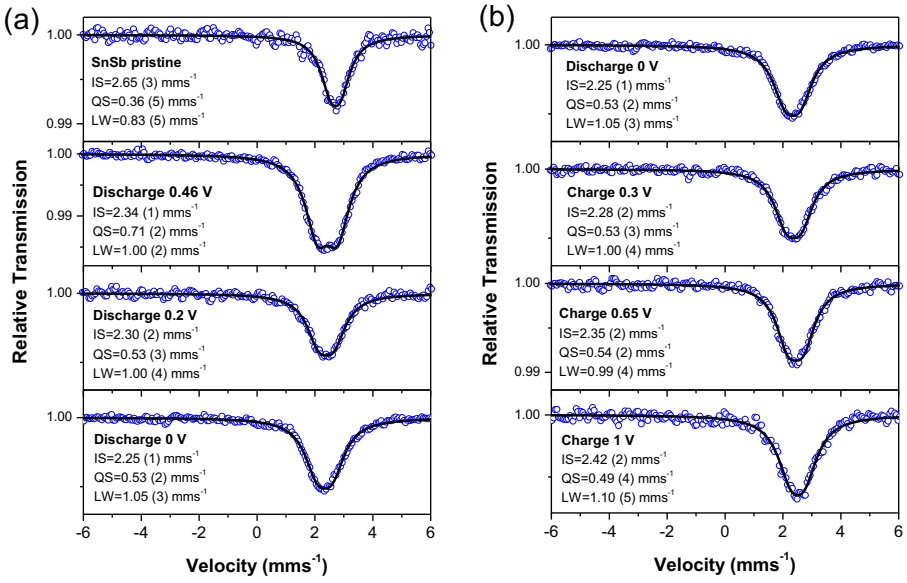

Fig. 7. Characterization of the reaction of SnSb with Na using ^{119}Sn Mössbauer spectroscopy during (a) discharge and (b) charge, corresponding to the positions highlighted by markers in Fig. 2.

situation results from the conversion of crystalline SnSb into an amorphous phase in which a significant amount of Na is remaining, as discussed earlier. Similar to the discharged electrodes, the quadrupole splitting values are relatively large, which we will discuss in detail in the next paragraph.

It is remarkable that the ^{119}Sn Mössbauer spectra systematically present fairly large quadrupole splitting values of about 0.5 mm s^{-1} or more. This result contrasts with the measurements of the starting material (0.36 mm s^{-1}) and those of Na-rich Na–Sn powder model compounds characterized by quadrupole splitting values of about 0.30–0.45 mm s^{-1} [3]. On the contrary, Sn thin film electrodes exhibit larger quadrupole splitting values of about 0.4–0.6 mm s^{-1} when amorphous phases are formed [3]. Hence, we attribute the larger splitting values to the formation of nanosized and/or amorphous Na_xSn phases, which possess some distribution of local environments as well as a relatively large surface to volume ratio.

The influence of nanosizing on the quadrupole splitting is a well-known property. In the case of the reaction of conversion anode tin nitride with Li, the fully discharged electrode was characterized by a ^{119}Sn isomer shift of 1.83 mm s^{-1} [24], which matched exactly with the value obtained for $Li_{21+5/16}Sn_5$ model compound [15,18]. However, this conversion electrode showed significantly larger quadrupole splitting values (~0.55 mm s^{-1}) with respect to the powder model compound (~0.30 mm s^{-1}) [15,18]. This phenomenon is also common to intermetallic systems in which a local extrusion process takes place during the reaction with Li or Na. For example, we recently evidenced that the reaction of Cu_2Sb with Na yields to the formation of Cu domains characterized by a significantly lower coordination number (6.7) than in bulk Cu (12) [9]. The formation of nanoparticles with average coordination numbers significantly smaller than for larger particles is well-recognized, and was studied using extended X-ray absorption fine structure (EXAFS) on, for instance, Ge nanoparticles of 4–9 nm average diameters [25]. For particles of 6 nm and less, the coordination number sharply decreased from about 3.70 to 3.65 and 3.30 for particle sizes of 6.0, 5.0 and 4.0 nm, respectively. Furthermore, the coordination number can be expected to decrease even faster for domains sizes smaller than 4 nm.

By analogy with these previous works, we think that the formation of Sn-rich and Sb-rich very fine domains is possible during the electrochemical reaction of SnSb with Na. These domains can exhibit a fair amount of Sn and Sb atoms present at the phase boundaries, which can lead to the presence of Sn and Sb coordination environments significantly different than those found in micron-sized particles. Within Na–Sn and Na–Sb model compounds, the complete surrounding of Sn or Sb atoms by Na tends to decrease the quadrupole splitting whereas the presence of Sn or Sb atoms in the vicinity of the probed atom increases the splitting [3,9]. Based on these considerations, the larger quadrupole splitting values measured here can suggest an increased number of Sn and Sb at the phase boundaries due to nanosizing.

4. Conclusions

We have discussed the structural properties of the products of Sb and SnSb thin films during the electrochemical reaction with Na using X-ray diffraction, ^{119}Sn and ^{121}Sb Mössbauer spectroscopies. The discharge (sodiation) of pure Sb starts with the formation of an amorphous phase composed of Sb atomic environments similar to those present in NaSb, and proceeds further by the formation of environments alike that of Na_3Sb. During charge, the reversible reaction takes place during a large portion of the process. The charged anode material, however, still contains a substantial fraction of Na, which can explain the lack of recrystallization into crystalline Sb. The reaction of SnSb yields Na_3Sb crystalline phase at full discharge at higher temperatures (65 and 95 °C) while the room temperature reaction proceeds with the formation of amorphous products. The electrochemically-driven, solid-state amorphization reaction occurring at room temperature is governed by the simultaneous formation of Na-coordinated Sn and Sb environments, as monitored by the decrease (increase) of the ^{119}Sn (^{121}Sb) Mössbauer isomer shifts. The absence of full sodiation of Sn environments is suggested by a ^{119}Sn isomer shift lower than those measured for Sn thin films or $Na_{15}Sn_4$ model compound. Moreover, the relatively large ^{119}Sn quadruple splitting values support the formation of nanosized domains with a broader distribution of coordination than in Na–Sn model compounds. The ^{119}Sn and ^{121}Sb isomer shift values further support the absence of full desodiation of SnSb during charge, in agreement with the reversible capacity obtained during the electrochemical measurements.

Acknowledgments

This work was supported by the U.S. Department of Energy (DOE), Basic Energy Sciences (BES), Materials Sciences and Engineering Division (LB, GMV). Microscopy research was supported via a user project supported by ORNL's Shared Research Equipment (ShaRE) User Program, which is also supported by DOE–BES. HYH, CEJ, JAJ would like to acknowledge the support of the Center for Laser Applications and the University of Tennessee Space Institute in relation with ^{121}Sb Mössbauer spectroscopy measurements. JCJ gratefully acknowledges Région Languedoc-Roussillon (France) for the financial support to the "X-rays and gamma-rays platform" of Université Montpellier II in relation with ^{119}Sn Mössbauer spectroscopy experiments.

Appendix A. Supplementary data

Supplementary data related to this article can be found at http://dx.doi.org/10.1016/j.jpowsour.2014.05.083.

References

[1] L.D. Ellis, T.D. Hatchard, M.N. Obrovac, J. Electrochem. Soc. 159 (2012) A1801–A1805.
[2] L. Baggetto, R.P. Meisner, P. Ganesh, R.R. Unocic, J.-C. Jumas, C.A. Bridges, G.M. Veith, J. Power Sources 234 (2013) 48–59.
[3] L. Baggetto, C.A. Bridges, J.-C. Jumas, D.R. Mullins, K.J. Carroll, R.A. Meisner, E.J. Crumlin, X. Liu, W. Yang, G.M. Veith, J. Mater. Chem. A (2014) unpublished.
[4] L. Baggetto, P. Ganesh, C.-N. Sun, R.A. Meisner, T.A. Zawodzinski, G.M. Veith, J. Mater. Chem. A 1 (2013) 7985–7994.
[5] A. Darwiche, C. Marino, M.T. Sougrati, B. Fraisse, L. Stievano, L. Monconduit, J. Am. Chem. Soc. 134 (2012) 20805–20811.
[6] A. Darwiche, M.T. Sougrati, B. Fraisse, L. Stievano, L. Monconduit, Electrochem. Commun. 32 (2013) 18–21.
[7] L. Xiao, Y. Cao, J. Xao, L. Kovarik, Z. Nie, J. Liu, Chem. Commun. 48 (2012) 3321–3323.
[8] L. Baggetto, J.-C. Jumas, J. Górka, C.A. Bridges, G.M. Veith, Phys. Chem. Chem. Phys. 15 (2013) 10885–10894.
[9] L. Baggetto, K.J. Carroll, H.-Y. Hah, C.E. Johnson, D.R. Mullins, R.R. Unocic, J.A. Johnson, Y.S. Meng, G.M. Veith, J. Phys. Chem. C 118 (2014) 7856–7864.
[10] L. Baggetto, E. Allcorn, A. Manthiram, G.M. Veith, Electrochem. Commun. 27 (2013) 168–171.
[11] D.-H. Nam, K.-S. Hong, S.-J. Lim, H.-S. Kwon, J. Power Sources 247 (2014) 423–427.
[12] L. Baggetto, M. Marszewski, J. Górka, M. Jaroniec, G.M. Veith, J. Power Sources 243 (2013) 699–705.
[13] L. Baggetto, E. Allcorn, R.R. Unocic, A. Manthiram, G.M. Veith, J. Mater. Chem. A 1 (2013) 11163–11169.
[14] L. Aldon, A. Garcia, J. Olivier-Fourcade, J.-C. Jumas, F.J. Fernández-Madrigal, P. Lavela, C. Pérez Vicente, J.-L. Tirado, J. Power Sources 119–121 (2003) 585–590.
[15] R.A. Dunlap, D.A. Small, D.D. MacNeil, M.N. Obrovac, J.R. Dahn, J. Alloys Compd. 289 (1999) 135–142.

[16] F.J. Fernández-Madrigal, P. Lavela, C. Pérez Vicente, J.L. Tirado, J.-C. Jumas, J. Olivier-Fourcade, Chem. Mater. 14 (2002) 2962–2968.
[17] S. Naille, J.-C. Jumas, P.-E. Lippens, J. Olivier-Fourcade, J. Power Sources 189 (2009) 814–817.
[18] F. Robert, P.-E. Lippens, J. Olivier-Fourcade, J.-C. Jumas, F. Gillot, M. Morcrette, J.-M. Tarascon, J. Solid State Chem. 180 (2007) 339–348.
[19] G.K. Shenoy, F.E. Wagner, G.M. Kalvius, in: G.K. Shenoy, F.E. Wagner (Eds.), Mössbauer Isomer Shifts, North-Holland Publishing Company, Amsterdam, New-York, Oxford, 1978, pp. 101–105.
[20] J.D. Donaldson, A. Kjekshus, D.G. Nicholson, M.J. Tricker, Acta Chem. Scand. 26 (1972) 3215–3225.
[21] L. Norén, R.L. Withers, S. Schmid, F.J. Brink, V. Ting, J. Solid State Chem. 179 (2006) 404–412.
[22] K. Kitadai, M. Takahashi, M. Takeda, J. Radioanal. Nucl. Chem. 255 (2003) 311–314.
[23] P.E. Lippens, Solid State Commun. 113 (2000) 399–403.
[24] L. Baggetto, J.-C. Jumas, H.T. Hintzen, P.H.L. Notten, 55 (2010) 6617–6631.
[25] L.L. Araujo, R. Giulian, D.J. Sprouster, C.S. Schnohr, D.J. Llewellyn, P. Kluth, Phys. Rev. B 78 (2008) 094112-1–094112-15.